Fundamental Aeroelastic Analysis of an Urban Air Mobility Rotor

Stephen J. Wright
Aerospace Engineer
NASA Ames Research Center
Moffet Field, CA, United States of America

ABSTRACT

A computational investigation was conducted of the aeroelastic characteristics of a representative rotor typical of aircraft for Urban Air Mobility. A rotorcraft comprehensive analysis was used to examine the aeroelastic characteristics of the model, both in hover and in forward flight. Throughout the study, parameters examined included rotor rotational speed, forward flight speed, blade torsion stiffness, and chordwise locations of the blade elastic axis and center of gravity. Three sets of airfoil properties were analyzed: NACA 0012, VR8, and VR12. For hover, the effect of dynamic inflow was studied via a comparison of uniform inflow and dynamic inflow models. Thrust coefficient and blade tip twist were analyzed to ascertain performance characteristics, and eigen analysis was employed to determine stability. For the forward flight cases, rpm and forward flight speed were swept separately, and the effect of each on performance and stability was assessed. Thrust coefficient and mean drag coefficient were used to evaluate performance of the rotor, and eigen analysis was invoked to study rotor stability. Forward flight stability results generated via a constant coefficient analysis were compared with results generated via Floquet Theory.

NOTATION

C_T/σ	=	thrust coefficient
C_D	=	drag coefficient
CG	=	center of gravity
EA	=	elastic axis
EI_{flap}	=	flap stiffness
EI_{lag}	=	lag stiffness
eVTOL	=	electric vertical take-off and landing
GJ	=	torsion stiffness
rev	=	revolution
rpm	=	revolutions per minute
R	=	rotor radius
UAM	=	urban air mobility
μ	=	advance ratio

INTRODUCTION

The frontier field of Urban Air Mobility (UAM) has yielded numerous, novel vertical lift aircraft. Many of these configurations boast non-traditional rotor types, many of which are designed to decrease weight and mechanical complexity. The push for reduced weight implies reduced blade stiffness and absence of mass balance about the blade quarter chord. This in turn implies significant elastic blade deflection, even for configurations without hinges or pitch bearings. The drive for efficiency has also led to the elimination of traditional load-alleviating and stability-enhancing features such as articulation. Additionally, many of the proposed designs vary rotor speed for thrust control, which poses challenges for vibrations and stability. Dynamical issues with UAM-type rotors were experimentally investigated in Ref. 1.

Of the numerous UAM vehicle concepts being put forth in industry, there are many combinations of fixed-pitch rotors, variable-rpm control systems, and stiff rotors in edgewise flight. The Volocopter VC200, a multicopter with 18 rotors, accomplishes all maneuvers via rpm control; each rotor can be adjusted independently of the other 17 (Ref. 2). The A^3 ~~A3~~ Vahana also has variable rpm capability, although it retains variable pitch blades (Ref. 2). Regarding rotors in edgewise flight, Aurora's vehicle is a good example. A prime example of a lift+cruise configuration, Aurora's electric vertical take-off and landing (eVTOL) aircraft has fixed pitch rotors for lift, and a wing/pusher prop for forward flight (Ref. 3).

This paper is an exploration of stability of a typical UAM-type rotor. The overall objective is to establish behaviors of concern and the impact of certain design parameters, such as blade torsion stiffness, chordwise offset of the blade center of gravity (CG) and elastic axis (EA), airfoil, rpm, and forward flight speed. This is by no means a comprehensive investigation. There are properties that were not studied, and for those that were, additional analysis will be necessary. The present paper serves only as a baseline for research in this particular field.

Presented at the Vertical Flight Society's 9th Biennial Autonomous VTOL Technical Meeting, Virtual, January 26-28, 2021.

APPROACH

The analysis of this study was conducted with the comprehensive rotorcraft analysis CAMRAD II (Ref. 4). CAMRAD II is an aeromechanics analysis of rotorcraft that incorporates a combination of advanced technologies including multibody dynamics, nonlinear finite elements, and rotorcraft aerodynamics. The trim task finds the equilibrium solution for a steady state operating condition and produces the solution for performance, loads, and vibration. The flutter task linearizes the equations about the trim solution and produces stability results.

This paper is organized as follows. First, the rotor model and its development are discussed and the nominal values of the blade properties are presented. Following this development, analysis results are presented in four sections. The first of these sections presents the results generated via an analysis of an isolated blade, in hover, with constant rotor inflow. For the hover analysis, rotor rotational speed swept. The second of these sections presents the results generated via a multiblade analysis of a hovering rotor with dynamic inflow. The third and fourth sections of results present the results generated via a multiblade analysis of a rotor in forward flight with dynamic inflow. For the forward flight cases, two different types of sweeps are run: wind speed sweeps and rotor rotational speed sweeps. The two forward flight sections differ in the type of analysis performed to obtain stability results. The third section uses averaged equations, while the fourth section presents results from an application of Floquet Theory. Floquet Theory is generally necessary for the assessment of cases of advance ratio in excess of ~0.5.

Throughout this paper, C_T/σ and mean drag coefficient plots are presented to reveal performance characteristics of the rotor, while eigen analysis results are presented to assess stability. For isolated blade analysis with uniform inflow, damping ratio plots are presented. For multibladed analysis, real eigenvalue components are plotted.

Stability-related predictions were generated via the CAMRAD II flutter solution. Automated mode tracking was not used in this study and thus, the linearized stability plots presented in this memorandum were manually created via visual inspection of data points.

ROTOR MODEL DEVELOPMENT

It was necessary to define a notional rotor with which to conduct the analysis. It was desired that the model would generically represent a rotor of the UAM genre, with a relatively small diameter, hingeless blades, and relatively soft-in-torsion stiffness properties. Rather than develop an entirely new configuration, a model was based on work already existing in the literature.

As described in Ref. 5, Johnson, Silva, and Solis published several UAM "reference vehicles." These concept models were built to be representative of the various features discovered in a survey of the UAM market. The concept vehicles were not intended for fabrication but were rather created to serve as generic baselines for research activities in the various technologies relevant to UAM vehicle design.

A quadrotor concept developed in Ref. 5 was chosen for the present study. This configuration has four, three-bladed, variable-collective rotors; the rotor radii are 6.94 ft (Ref. 5). Only a single rotor was analyzed for the present study. While the rotor model created in Ref. 5 was developed sufficiently for design purposes, for this study, the rotor properties were simplified for the purpose of streamlining the analysis and generalizing the results. The taper of the quadrotor was eliminated, yielding a rectangular planform. The linear twist was maintained. The chord length was derived from a desired geometric solidity ratio of 0.12.

Rather than developing blade stiffness properties via an in-depth sectional design, the nominal values for the flap, lag, and torsional stiffnesses were defined such that the rotor operating at its nominal rpm with EA and CG both at the quarter chord had approximately 1.5/rev, 2.5/rev, and 4/rev as its fundamental flap, lag, and pitch frequencies, respectively. Inertial properties were derived to yield a Lock Number of approximately 5.0. Table 1 presents the nominal rotor properties. Of the listed values, only GJ was varied during the scope of this work.

Table 1. Rotor Properties

Characteristic	Value
Chord	0.8721 ft
Radius	6.94 ft
Solidity	0.12
Number of Blades	3
Linear Twist	-13 deg
Blade Pitch (75%R)	10 deg
Nominal Rotor Rotational Speed	700 rpm
Nominal Tip Speed	508. 73 ft/s
Nominal Tip Mach Number	0.4557
Design C_T/σ	0.067
EI_{lag}	0.5E+6 lb-ft^2
EI_{flap}	0.1E+6 lb-ft^2
Nominal GJ	1000 lb-ft^2
Torsion Frequency (GJ=1000 lb-ft^2)	5.2804 per rev
Torsion Frequency (GJ=2000 lb-ft^2)	7.3001 per rev
Torsion Frequency (GJ=3000 lb-ft^2)	8.8728 per rev
Torsion Frequency (GJ=4000 lb-ft^2)	10.2085 per rev
Torsion Frequency (GJ=5000 lb-ft^2)	11.3869 per rev
Structural Damping	0.5% critical
Section Mass	0.34142 slug/ft
Section Moment of Inertia	1.1847 slug-ft^2/ft
Lock Number	5.0

The exploration of different airfoils was limited to three airfoils: NACA 0012 (Ref. 6), VR8, and VR12. The NACA 0012 is a classic rotor airfoil and is being used for some

UAVs. Because it is a commonly studied symmetric airfoil, it was chosen as the starting point for the present work. The VR8 (Refs. 7-8) and VR12 (Ref. 9) are more modern than the NACA 0012 and are both cambered airfoils; the camber impacts pitch moment and stall. The VR8 was designed primarily for hover, while the VR12 was designed primarily for forward flight. Thus, despite the limitation of only analyzing three airfoils in this work, the choice of the NACA 0012, VR8, and VR12 captures a decent variety of airfoil characteristics.

HOVER | UNIFORM INFLOW

For this study, four different parameters were examined for their impact on rotor stability. These four parameters were airfoil, EA/CG location, GJ, and rpm. The results are broken into three sections, with one section devoted to each airfoil. Within these three sections are two subsections, one each for the two different configurations of EA/CG that were examined. C_T/σ vs rotor rotational speed is plotted to illustrate performance characteristics. Damping ratio vs rotor rotational speed is plotted to illustrate the dynamic stability of the system. For configurations with the EA/CG at 25% chord, damping ratio plots are included for any unstable modes (or the modal analogue for the dynamically-stable cases). For configurations with the EA/CG at 35% chord, a table is presented with the flutter speeds of the critical modes.

NACA 0012 Airfoil with EA/CG at 25% Chord

For this combination of configuration and airfoil, all five torsion stiffness values yield acceptable C_T/σ values within the design rpm envelope. As displayed in Fig. 1, for all five values of GJ, there is a significant drop in C_T/σ between 1000 and 1300 rpm. Note that the legend in Fig. 1 applies to Figs. 1-5. Figure 2 shows that the decrease in C_T/σ is due to nose-down pitch of the NACA 0012 airfoil at elevated tip speed.

The plot of thrust coefficient suggests that GJ values of 1000, 2000, 3000, 4000, and 5000 lb-ft^2, are all acceptable below approximately 1100 rpm. However, the eigen analysis presented in Fig. 3 shows that the blade flutters for GJ values of 1000 and 2000 lb-ft^2. With GJ of 1000 lb-ft^2, the flutter boundary is approximately 700 rpm. For GJ of 2000 lb-ft^2, the flutter boundary is approximately 1100 rpm. Note that the effect of GJ is nonlinear, with little effect above 4000 lb-ft^2.

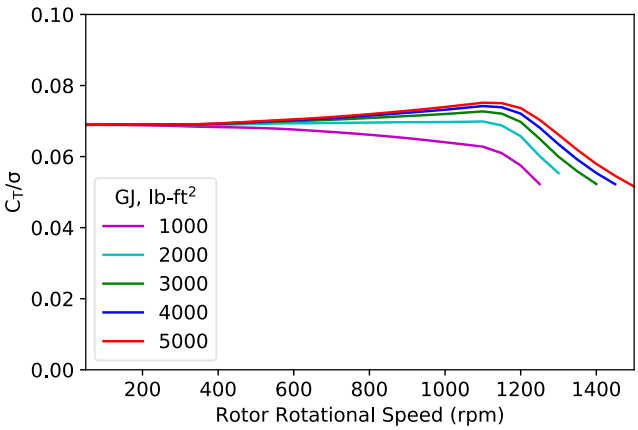

Figure 1. C_T/σ vs rpm, NACA 0012, EA/CG at 25% chord, five values of GJ

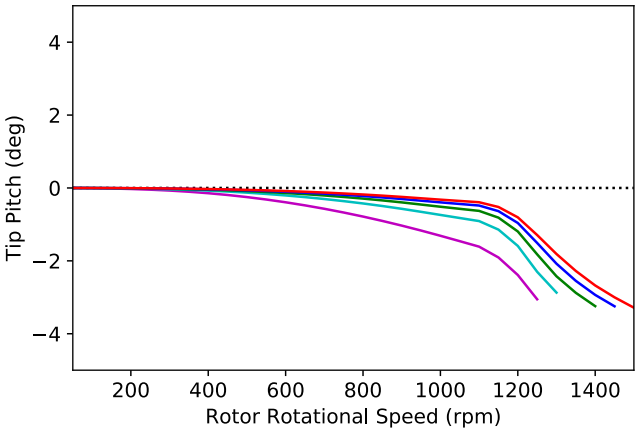

Figure 2. Tip pitch vs rpm, NACA 0012, EA/CG at 25% chord, five values of GJ

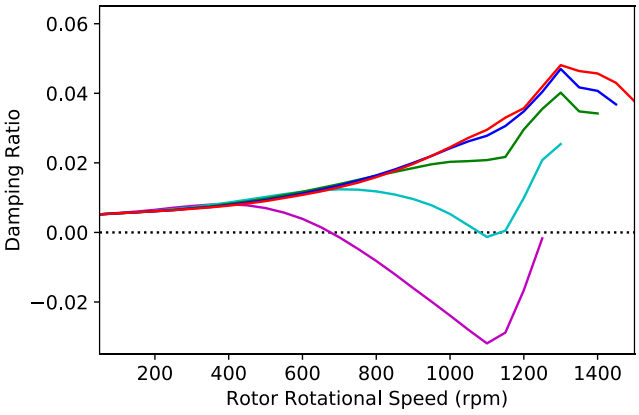

Figure 3. Damping ratio vs rpm, NACA 0012, EA/CG at 25% chord, five values of GJ

NACA 0012 Airfoil with EA/CG at 35% Chord

Figure 4 shows that, even with GJ of 5000 lb-ft^2, the rotor stalls around 700 rpm (approximately the design speed). The dramatic, approximately exponential, growth of C_T/σ prior to stall is indicative of increase in blade pitch. This is confirmed by Fig. 5, which plots tip pitch vs rpm for each value of GJ.

Figure 6 plots damping ratio vs rpm for the case of nominal torsion stiffness. Note that the six lines in Fig. 6 represent the six unstable modes of the nominal GJ case. Table 2 summarizes the flutter speeds of the critical modes for cases with GJ values of 1000-5000 lb-ft^2. Note that these tabulated flutter rpm values are approximate. Rotor rpm was swept in increments of 50; the values shown in Table 2 are the average of the highest stable rpm value and the lowest unstable rpm value for each respective case set. Clearly, this configuration is not suitable with the analyzed values of GJ, but several observations may be made. A blade with stiffer-in-torsion properties may be capable of operating with this airfoil/structural axes combination; however, other GJ values were not explored as a part of this work. Comparing Figs. 4 and 6, it can be seen that for one of the modes, an abrupt drop in damping ratio coincides with the stall point. This is the result of a loss in flap damping that occurs when most of the blade is stalled. As expected, the rearward shift of the CG/EA severely detracts from the efficacy of the rotor configuration.

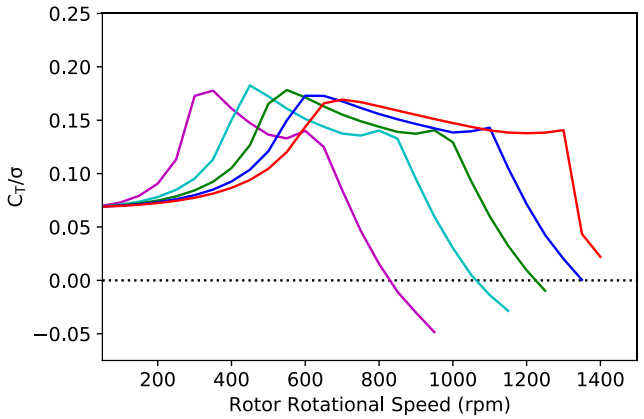

Figure 4. C_T/σ vs rpm, NACA 0012, EA/CG at 35% chord, five values of GJ

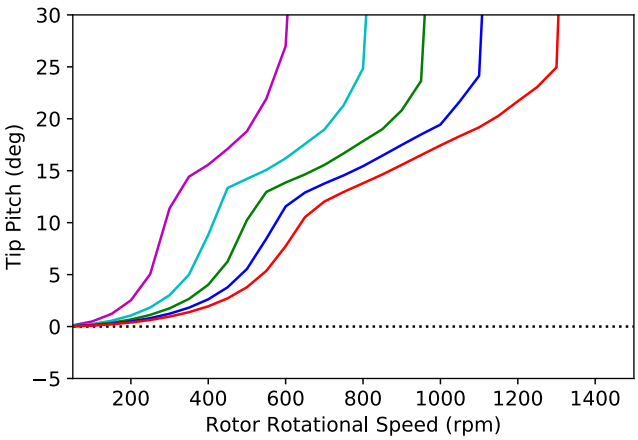

Figure 5. Blade tip pitch vs rpm, NACA 0012, EA/CG at 35% chord, five values of GJ

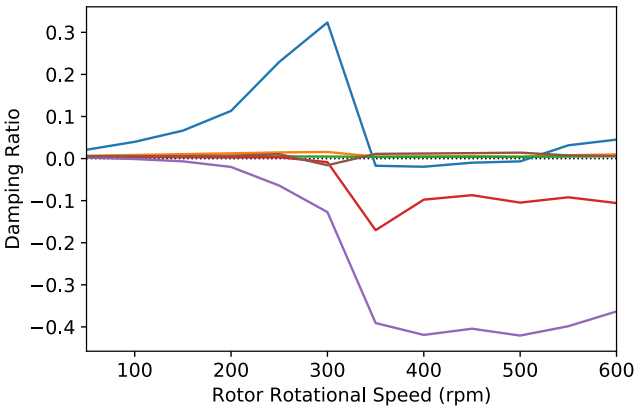

Figure 6. Damping ratio vs rpm, NACA 0012, EA/CG at 35% chord, GJ=1000 lb-ft^2

Table 2. Flutter Speed, EA/CG at 35% Chord

Airfoil	GJ (lb-ft^2)	Flutter Speed (rpm)
NACA 0012	1000	75
NACA 0012	2000	125
NACA 0012	3000	175
NACA 0012	4000	275
NACA 0012	5000	475

VR8 Airfoil with EA/CG at 25% Chord

Figure 7 shows C_T/σ vs rotor rotational speed for the VR8 airfoil. Note that the legend of Fig. 7 applies to Figs. 7-11. With GJ values of 3000, 4000, and 5000 lb-ft^2, a dramatic drop of C_T/σ occurs at approximately 1200 rpm. The lesser GJ values do not have the sharp decrease in C_T/σ, but rather experience a steady decrease in the quantity, leading to the determination that such torsion stiffness values are inadequate for the configuration. As with the NACA 0012 case with the EA and CG at 25% chord, the drop of C_T/σ is due to nose-down pitch, as indicated by Fig. 8.

Figure 9 displays damping ratio vs rotor rotational speed. For GJ values of 1000-5000 lb-ft^2, the blade is dynamically

stable, as there is no crossing of the zero-damping axis. This is a marked difference from the analogous NACA 0012 configuration, for which both GJ values of 1000 and 2000 lb-ft^2 resulted in flutter.

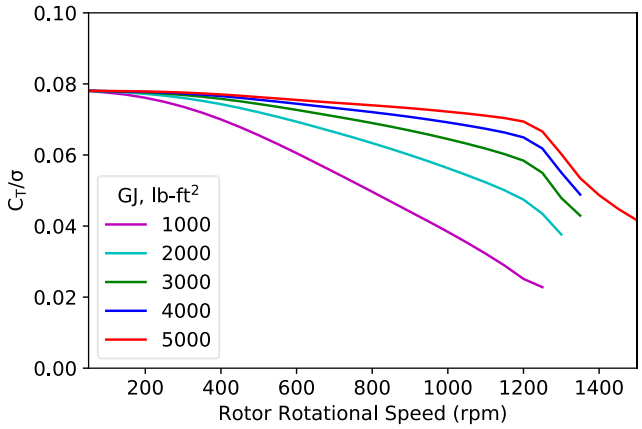

Figure 7. C_T/σ vs rpm, VR8, EA/CG at 25% chord, five values of GJ

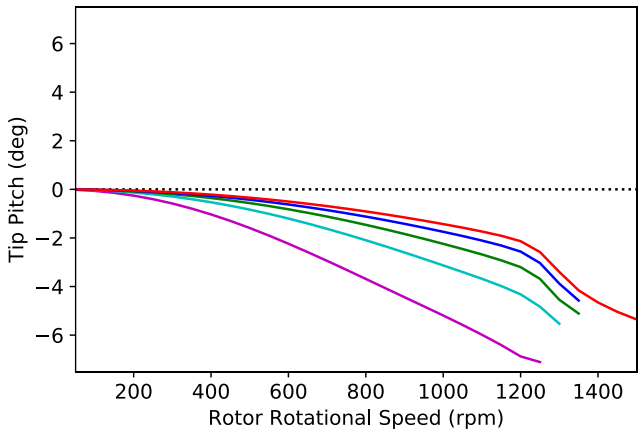

Figure 8. Blade tip pitch vs rpm, VR8, EA/CG at 25% chord, five values of GJ

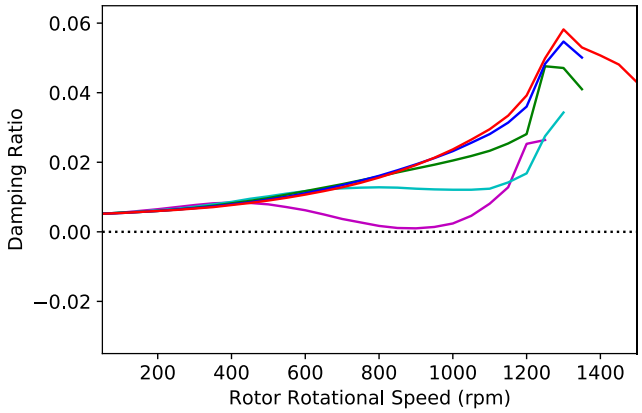

Figure 9. Damping ratio vs rpm, VR8, EA/CG at 25% chord, five values of GJ

VR8 Airfoil with EA/CG at 35% Chord

The rearward shift of the EA/CG with the VR8 airfoil yielded similar results to the analogous cases with the NACA 0012. Figure 10 is a plot of C_T/σ vs rpm, and Fig. 11 is a plot of blade tip pitch vs rpm. Table 3 summarizes the flutter rpm for all analyzed GJ values (1000–5000 lb-ft^2). Multiple modes fluttered; however, Table 3 presents only the flutter speeds of the critical modes. Both stall speeds and flutter speeds render these combinations of airfoil/configuration/stiffness unsuitable for the application. Blades with higher torsion stiffness may be a solution, but as was mentioned in the NACA 0012 section, higher values were not investigated in the present study.

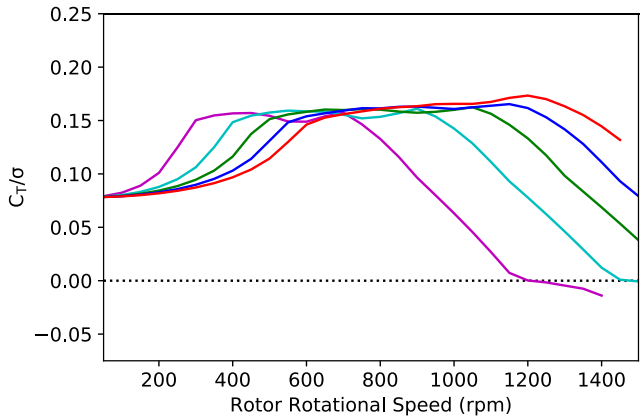

Figure 10. C_T/σ vs rpm, VR8, EA/CG at 35% chord, five values of GJ

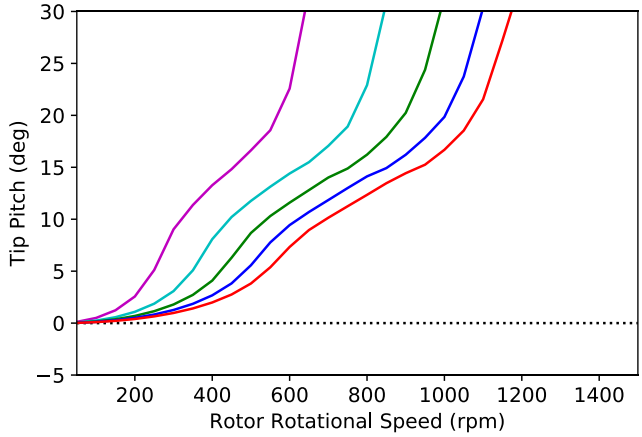

Figure 11. Blade tip pitch vs rpm, VR8, EA/CG at 35% chord, five values of GJ

Table 3. Flutter Speed, EA/CG at 35% Chord

Airfoil	GJ (lb-ft^2)	Flutter Speed (rpm)
VR8	1000	75
VR8	2000	75
VR8	3000	125
VR8	4000	125
VR8	5000	175

VR12 Airfoil with EA/CG at 25% Chord

The analysis of the previous subsections was repeated with the VR12 airfoil. A similar story resulted. As shown in Figs. 12-13, lower GJ values lead to a drop in C_T/σ due to nose-down pitch. Note that the legend in Fig. 12 applies to Figs. 12-16.

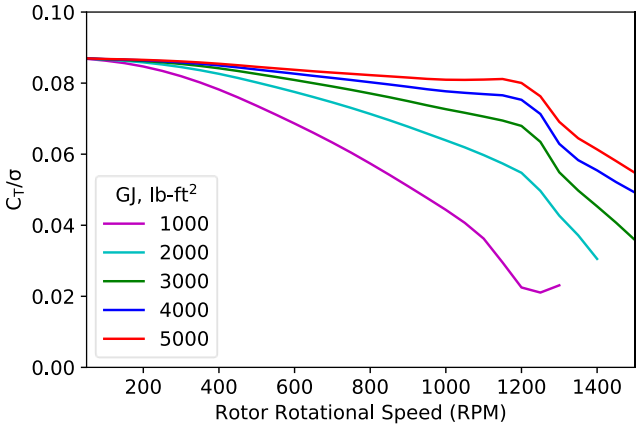

Figure 12. C_T/σ vs rpm, VR12, EA/CG at 25% chord, five values of GJ

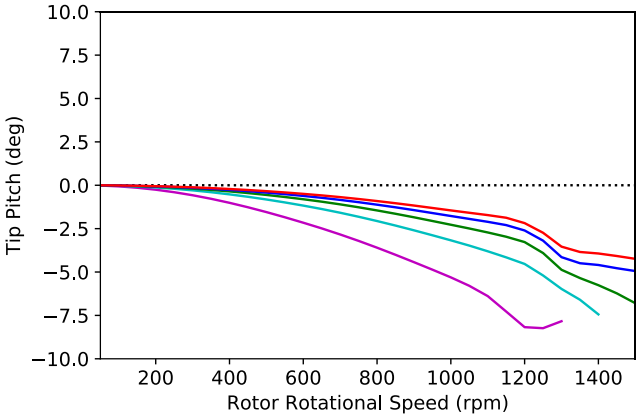

Figure 13. Tip pitch vs rpm, VR12, EA/CG at 25% chord, five values of GJ

Considering only the dynamic stability as presented in Fig. 14 for a nominal rotor rotational speed of 700 rpm, this configuration is dynamically stable for all GJ values; however, if rpm is to be used as a means of control, the 800 rpm flutter speed for the GJ=1000 lb-ft^2 case may not provide enough margin.

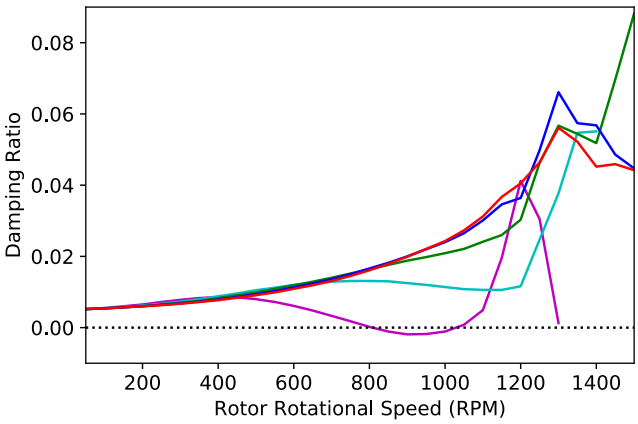

Figure 14. Damping ratio vs rpm, VR12, EA/CG at 25% chord, five values of GJ

VR12 Airfoil with EA/CG at 35% Chord

As with the NACA 0012 and VR8, the rearward shift of the EA/CG has serious negative repercussions, both regarding performance and stability. Figure 15 shows that the blade has unacceptable stall characteristics for all values of GJ. As with the other airfoils, the quasi-exponential growth of C_T/σ is indicative of severe coupling of blade twist and rotor rotational speed (see Fig. 16). Even neglecting stall, this configuration is unacceptable from the perspective of dynamic stability. Table 4 tabulates the critical mode flutter speed for cases with GJ of 1000-5000 lb-ft^2. All GJ values yield flutter speeds well below the desired nominal rotor speed of 700 rpm. Note that in Fig. 16, the truncation of the 2000 and 3000 lb-ft^2 cases resulted from convergence problems with the CAMRAD II analysis. These numerical issues were ignored as they occurred beyond the flutter points.

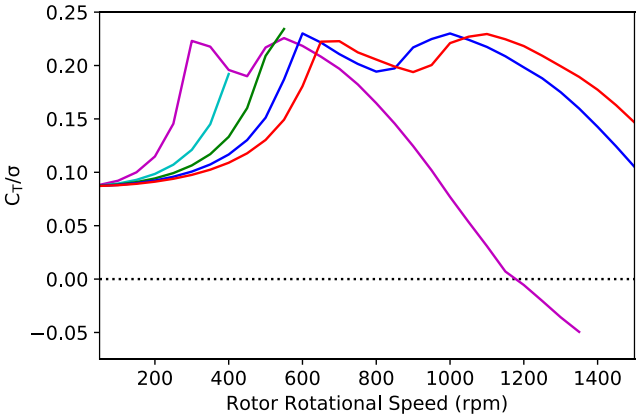

Figure 15. C_T/σ vs rpm, VR12, EA/CG at 35% chord, five values of GJ

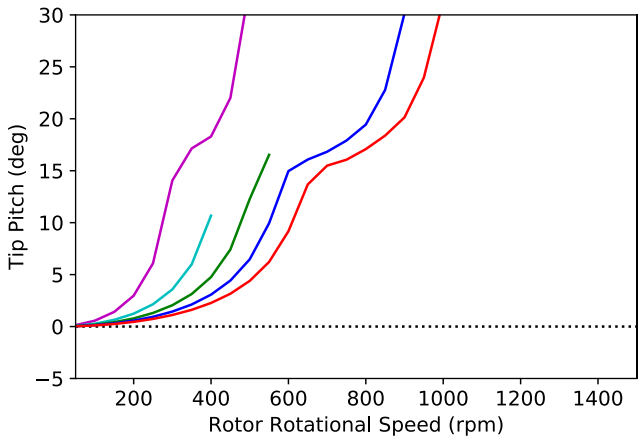

Figure 16. Tip pitch vs rpm, VR12, EA/CG at 35% chord, five values of GJ

Table 4. Flutter Speed, EA/CG at 35% Chord

Airfoil	GJ (lb-ft^2)	Flutter Speed (rpm)
VR12	1000	125
VR12	2000	175
VR12	3000	325
VR12	4000	425
VR12	5000	525

HOVER | DYNAMIC INFLOW

This section replicates the previous section but with dynamic inflow instead of uniform inflow. This is a far more realistic condition because the impact of the wake on the blade loading is significant, especially for hover with wake below the blades. Multiblade coordinates are necessary for the analysis since dynamic inflow couples all blades in the nonrotating frame. While the previous stability results were plotted as damping ratio vs rpm, for multiblade coordinates, stability is plotted as the real eigenvalue component vs rpm. In changing from plots of damping ratio to plots of eigenvalue components, there is also a change in sign; instability is identified by a *negative* damping ratio but by a *positive* real eigenvalue component.

NACA 0012 Airfoil with EA/CG at 25% Chord

The plot of thrust coefficient shown in Fig. 17 is much the same as the analogous plot from the uniform inflow cases (Fig. 1). Note that the legend of Fig. 17 applies to Figs. 17-19. For all five values of GJ, C_T/σ dropped substantially between 1100 and 1200 rpm due to nose-down pitch, as shown in Figs. 17-18.

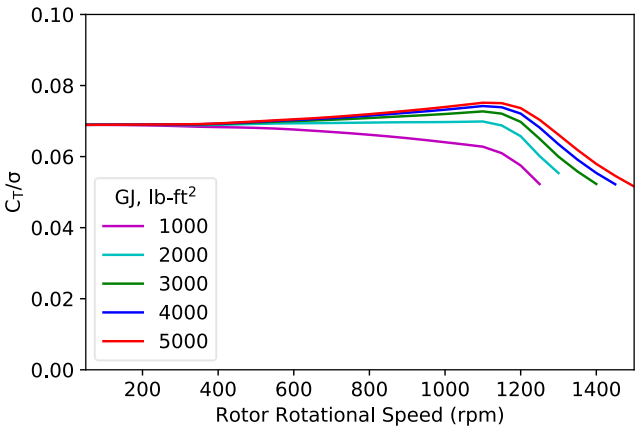

Figure 17. C_T/σ vs rpm, NACA 0012, EA/CG at 25% chord, five values of GJ

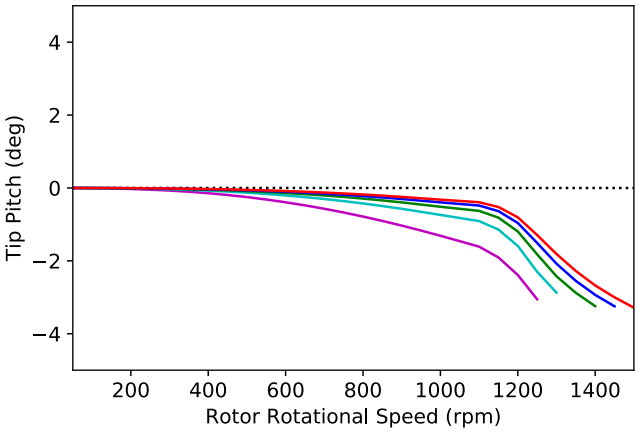

Figure 18. Tip pitch vs rpm, NACA 0012, EA/CG at 25% chord, five values of GJ

While the C_T/σ plot for this configuration is nearly identical between the uniform and dynamic inflow cases (compare Figs. 1 and 17), the same is not true for the results of the eigen analysis. With uniform inflow, the damping ratio plot shows that the blade flutters for both GJ of 1000 and 2000 lb-ft^2 (Fig. 3). The analogous plot for the dynamic inflow analysis is Fig., 19, which plots the real component of the eigenvalue vs rotational speed. Note that there are three lines of each color, representing three lines for each value of GJ (colors defined in legend of Fig. 17). This is due to the effect of dynamic inflow with the multiblade analysis (three-bladed rotor). For this configuration *with dynamic inflow*, GJ of 2000 lb-ft^2 yields a dynamically stable system. Only GJ of 1000 lb-ft^2 results in flutter. In this sense, the dynamic inflow has a stabilizing effect.

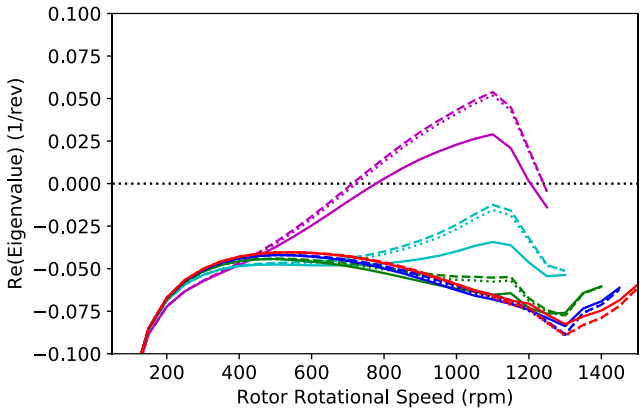

Figure 19. Stability vs rpm, NACA 0012, EA/CG at 25% chord, five values of GJ

NACA 0012 Airfoil with EA/CG at 35% Chord

From Figs. 20-21, it can be deduced that excessive elastic twist of the blade yields significant stall on the blades. Note that the legend of Fig. 20 applies to Figs. 20-21. As shown in Fig. 21, this stall is due to excessive, nose-up elastic twist of the blade For none of the five analyzed values of GJ is the C_T/σ indicative of a rotor suitable for operation at the nominal speed of 700 rpm. Table 5 tabulates the critical flutter speeds for this configuration for GJ values of 1000-5000 lb-ft^2. As with the uniform inflow case, the aftward shift of the EA/CG had a negative impact both on performance and on stability.

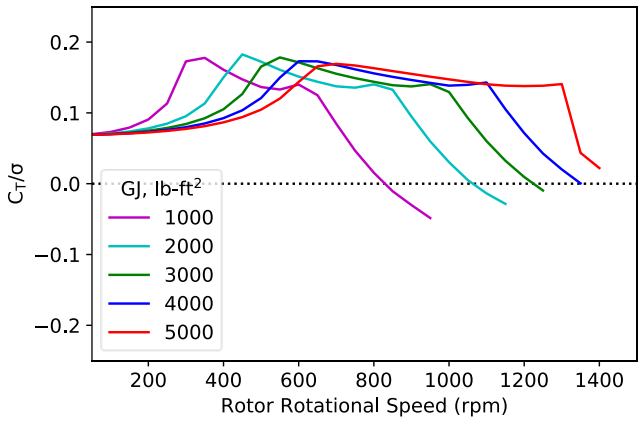

Figure 20. C_T/σ vs rpm, NACA 0012, EA/CG at 35% chord, five values of GJ

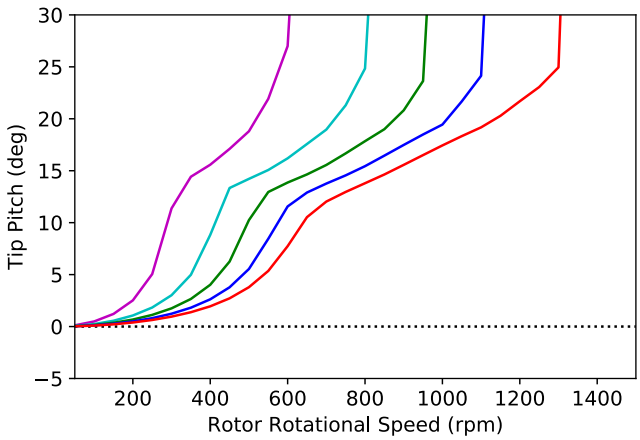

Figure 21. Blade tip pitch vs rpm, NACA 0012, EA/CG at 35% chord, five values of GJ

Table 5. Flutter Speed, EA/CG at 35% Chord

Airfoil	GJ (lb-ft^2)	Flutter Speed (rpm)
NACA 0102	1000	75
NACA 0102	2000	125
NACA 0102	3000	125
NACA 0102	4000	175
NACA 0102	5000	225

VR8 Airfoil with EA/CG at 25% Chord

Figure 22 displays that, for GJ of 5000 lb-ft^2, this configuration experiences a drop in C_T/σ at approximately 1200 rpm. Note that the legend of Fig. 22 applies to Figs. 22-24. Figure 23, which displays blade tip pitch, indicates that this loss of C_T/σ is due to nose-down elastic twist of the blade. For all analyzed values of torsion stiffness, C_T/σ decreases with increasing rotor rotational speed, although for the lower GJ cases, the rate of decrease is of greater magnitude.

The results of the eigen analysis, displayed in Fig. 24, show that for 50-1500 rpm the rotor does not flutter for any of the analyzed values of GJ. Unsurprisingly, GJ of 1000 lb-ft^2 most nearly approached the flutter boundary; however, stability was maintained. Thus, for this configuration, performance, and not stability, is the limiting factor.

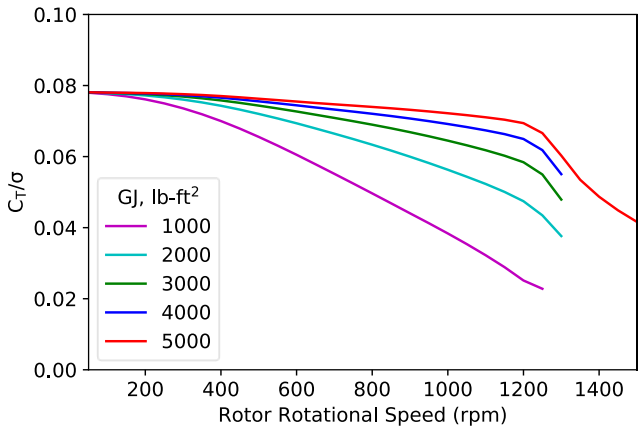

Figure 22. C_T/σ vs rpm, VR8, EA/CG at 25% chord, five values of GJ

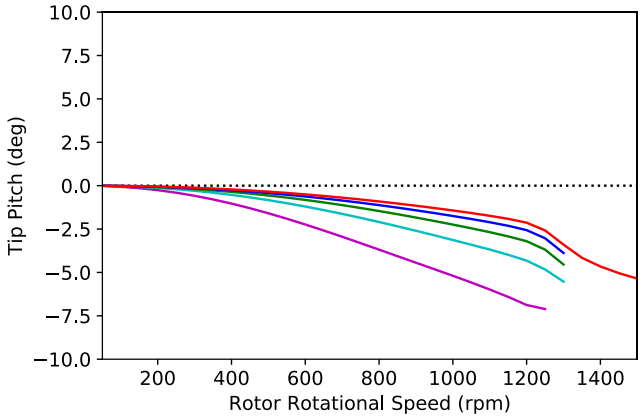

Figure 23. Tip pitch vs rpm, VR8, EA/CG at 25% chord, five values of GJ

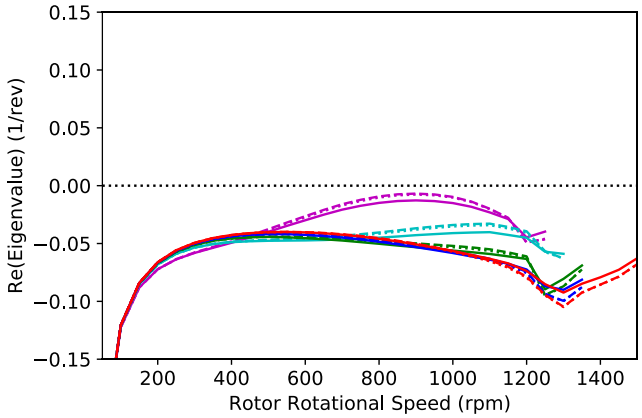

Figure 24. Stability vs rpm, VR8, EA/CG at 25% chord, five values of GJ

VR8 Airfoil with EA/CG at 35% Chord

From Figs. 25-26, it can be deduced that excessive elastic twist of the blade results in blade stall. Note that the legend of Fig. 25 applies to Figs. 25-26. Table 6 tabulates the critical mode flutter speeds for this configuration for GJ values of 1000-5000 lb-ft^2. From a stability perspective, this configuration performs extremely poorly.

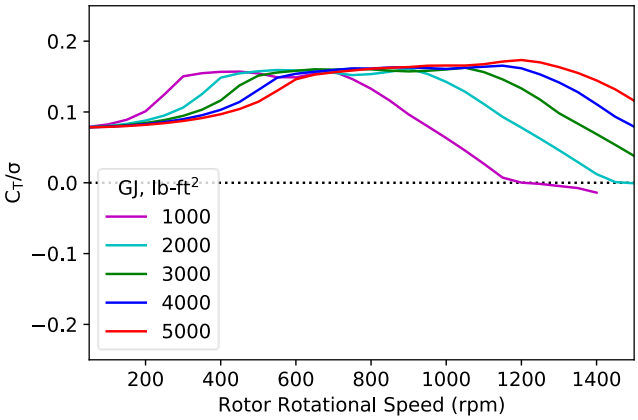

Figure 25. C_T/σ vs rpm, VR8, EA/CG at 35% chord, five values of GJ

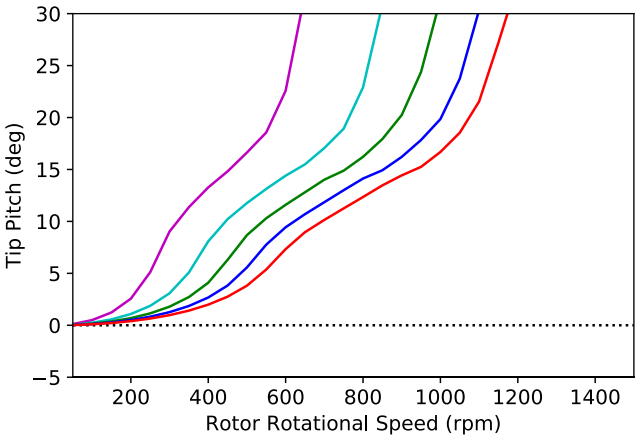

Figure 26. Blade tip pitch vs rpm, VR8, EA/CG at 35% chord, five values of GJ

Table 6. Flutter Speed, EA/CG at 35% Chord

Airfoil	GJ (lb-ft^2)	Flutter Speed (rpm)
VR8	1000	75
VR8	2000	75
VR8	3000	125
VR8	4000	125
VR8	5000	125

VR12 Airfoil with EA/CG at 25% Chord

The C_T/σ plot presented in Fig. 27 is similar to the analogous plot for the VR8 with uniform inflow (Fig. 10). Note that the legend of Fig. 27 applies to Figs. 27-29. Drop in C_T/σ corresponds to nose-down blade twist, as shown in Fig. 28. The plot of the real eigenvalue components (Fig. 29) is also similar between the VR8 and VR12. Neither airfoil flutters; however, for the case with GJ of 1000 lb-ft^2, the stability margin is noticeably greater for the VR8 than for the VR12.

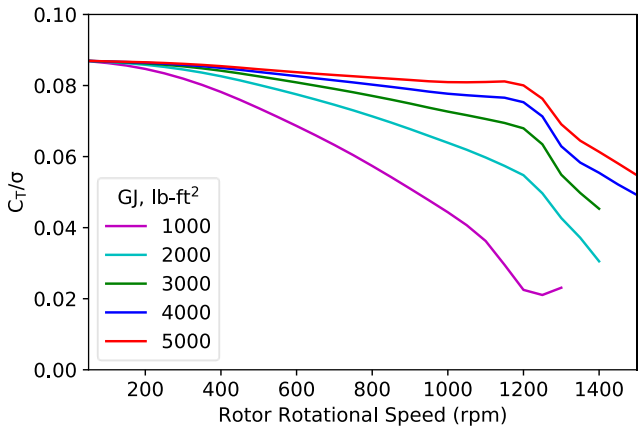

Figure 27. C_T/σ vs rpm, VR12, EA/CG at 25% chord, five values of GJ

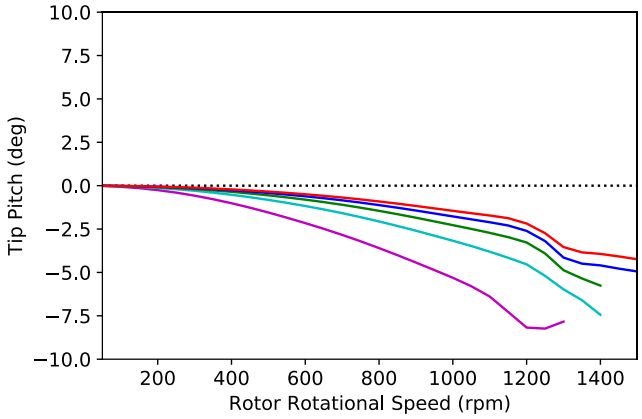

Figure 28. Tip pitch vs rpm, VR12, EA/CG at 25% chord, five values of GJ

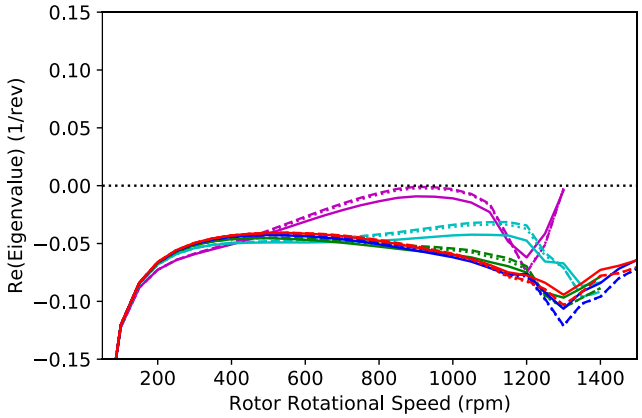

Figure 29. Stability vs rpm, VR12, EA/CG at 25% chord, five values of GJ

VR12 Airfoil with EA/CG at 35% Chord

From Figs. 30-31, it can be deduced that excessive elastic twist of the blade results in blade stall. Note that the legend of Fig. 30 applies to Figs. 30-31. For none of the five analyzed values of GJ is the C_T/σ indicative of a rotor suitable for operation at the nominal speed of 700 rpm. From a stability perspective, this configuration performs extremely poorly. Table 7 summarizes the flutter speeds for GJ of 1000-5000 lb-ft^2. Flutter speeds are well below the nominal rotor rotational speed, even for GJ of 5000 lb-ft^2.

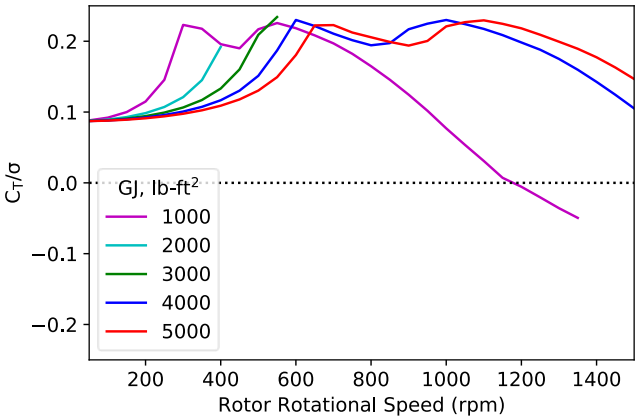

Figure 30. C_T/σ vs rpm, VR12, EA/CG at 35% chord, five values of GJ

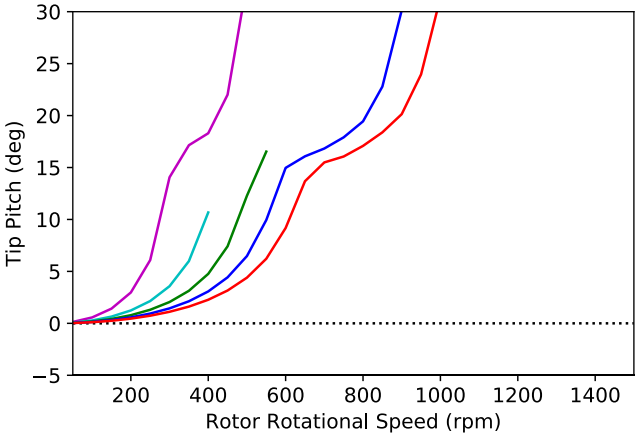

Figure 31. Blade tip pitch vs rpm, VR12, EA/CG at 35% chord, five values of GJ

Table 7. Flutter Speed, EA/CG at 35% Chord

Airfoil	GJ (lb-ft^2)	Flutter Speed (rpm)
VR12	1000	75
VR12	2000	125
VR12	3000	175
VR12	4000	275
VR12	5000	425

HOVER CONCLUSIONS

For all configurations, elevated rotor speed led to dramatic drop in C_T/σ. This was due to elastic blade twisting (nose-down for EA/CG at 25% chord and nose-up for EA/CG at 35% chord), and thus a stiffer blade would be necessary.

Figure 32 summarizes the flutter speeds for the hover cases analyzed with uniform inflow. As can be seen, no

airfoil/stiffness combination studied yielded an acceptable flutter speed when the EA/CG was shifted from the 25% chord to 35% chord. Note that the VR8 with EA/CG at 25% chord is not shown; that case did not flutter within the analyzed range of rpm.

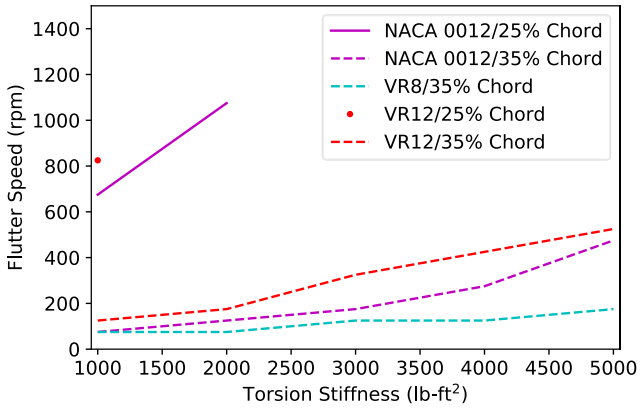

Figure 32. Flutter rpm vs torsion stiffness. Hover with isolated blade and uniform inflow

Figure 33 summarizes the flutter speeds for the hover cases analyzed with dynamic inflow. As can be seen, no airfoil/stiffness combination studied yielded an acceptable flutter speed when the EA/CG was shifted from the 25% chord to 35% chord. Note that the VR8 and VR12 with EA/CG at 25% chord did not flutter within the analyzed range of rpm.

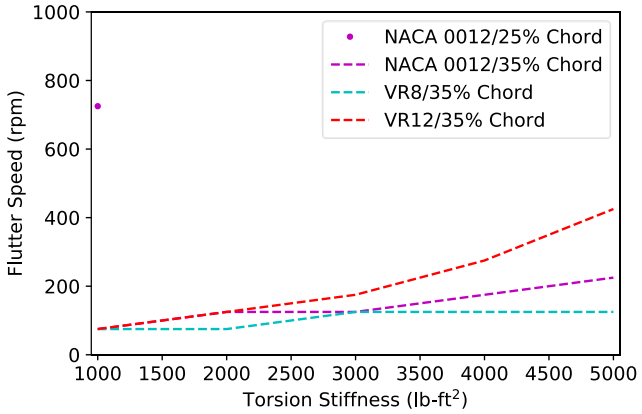

Figure 33. Flutter rpm vs torsion stiffness. Hover with multiblade coordinates and dynamic inflow

Figures 32-33 highlight the dependency of stability on blade stiffness and airfoil. Stiffer blades flutter at higher values of rotor rotational speed, and increased stiffness has a greater effect on flutter speed for the NACA 0012 and VR12 than for the VR8.

Figures 32-33 also show that the rearward shift of the EA/CG poses a significant problem for stability. This is concerning, as an EA/CG location of 35% chord is not necessarily extreme. One potential mitigation is increased stiffness; however, as implied by Figs. 32-33, such a stiffness must be in excess of the maximum analyzed in this work.

Figure 34 compares uniform and dynamic inflow analysis. Flutter speed for all three airfoils with EA/CG at 35% chord is plotted against GJ. An analogous plot was not created for the 25% chord configuration due to the overall stability of the analyzed conditions. Solid lines represent uniform inflow and isolated blade analysis, while dashed lines represent dynamic inflow with multiblade analysis.

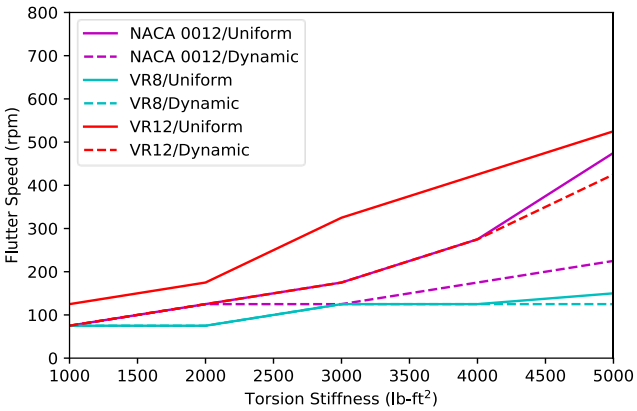

Figure 34. Flutter speed vs torsion stiffness, EA/CG at 35% chord. Comparison of uniform and dynamic inflow models

This plot reveals that for this configuration, dynamic inflow yields a flutter speed less than or equal to that for uniform inflow. It can be concluded that for this configuration, regardless of inflow type, the VR12 has the highest flutter speed, followed by the NACA 0012 and then the VR8. This should not be taken as a recommendation for the use of VR12 airfoils; rather, this observation should illustrate the importance of airfoil choice and its ramifications on the resulting stability boundaries and necessary blade stiffnesses.

FORWARD FLIGHT

All previous analysis was conducted with hover conditions (uniaxial flow). The analysis presented in this section was conducted with non-zero forward flight speed. Note that while not in hover, the shaft axes remained perpendicular to the flow. This is representative of a vehicle configuration that employs separate propulsors for lift and forward thrust.

Due to the increased complexity of forward flight analysis and the addition of a new variable parameter (flight speed), not all configuration/airfoil combinations from previous sections were repeated; instead, a subset of those cases was analyzed.

Table 8 provides the parameters used for the forward flight scope of work. A triplet of the form x:y:z indicates a sweep of a given parameter, for which “x” is the minimum value, “y” is the maximum value, and “z” is the increment size.

Table 8. Parameters for Forward Flight Study

Characteristic	Value
EA	25% or chord
CG	25% of chord
GJ	1000:5000:1000 lb-ft2
Airfoil	NACA 0012, VR8, VR12
Rotor Rotational Speed	700 and 50:1500:50 rpm
Wind speed	0:200:10 and 100

Within the 0-200 knot speed sweep, a nominal rotor speed of 700 rpm was maintained. At 100 knots, a 50:1500:50 rpm sweep was conducted.

NACA 0012 AIRFOIL, PERFORMANCE ANALYSIS

Figure 35 is a plot of mean drag coefficient (Mean C_D) vs advance ratio (the legend in Fig. 35 applies to Figs. 35-38). The rotor speed is fixed at 700 rpm and the wind speed is swept. Figure 36 again plots Mean C_D vs advance ratio, but as a 50:1500:50 rpm sweep of rotor rotational speed wind speed fixed at 100 knots).

In general, a doubling of Mean C_D indicates significant stall on the retreating side of the rotor disk. Applying this assumption to Fig 35, it can be inferred that for the nominal GJ value of 1000 lb-ft^2 and the nominal rotor speed of 700 rpm, significant stall is built up by an approximate advance ratio of 0.6. This advance ratio is lower for the higher GJ cases; the 5000 lb-ft^2 case stalls at an advance ratio of approximately 0.4.

Figure 37 shows the relationship between thrust coefficient and advance ratio with rpm fixed at 700. Torsion stiffness has a noticeable effect on this relationship. Figure 38 shows the relationship between thrust coefficient vs advance ratio at 100 kts. For this latter case, torsion stiffness has very little effect on both the nature of the relationship and on the values of thrust coefficient.

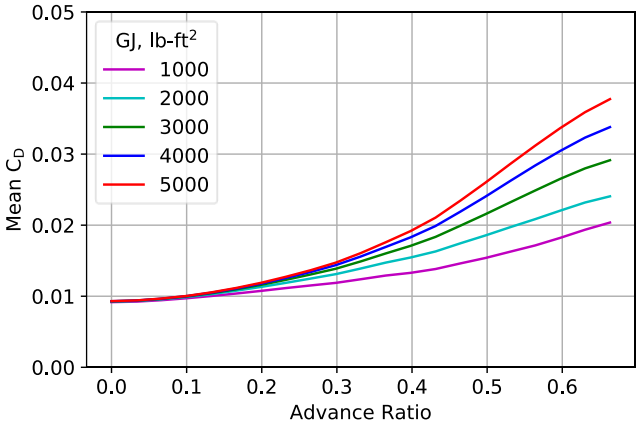

Figure 35. Mean C_D vs advance ratio (700 rpm), NACA 0012, five values of GJ

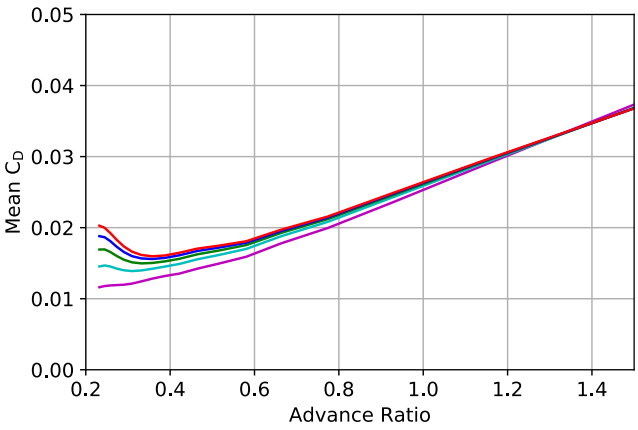

Figure 36. Mean C_D vs advance ratio (100 kts), NACA 0012

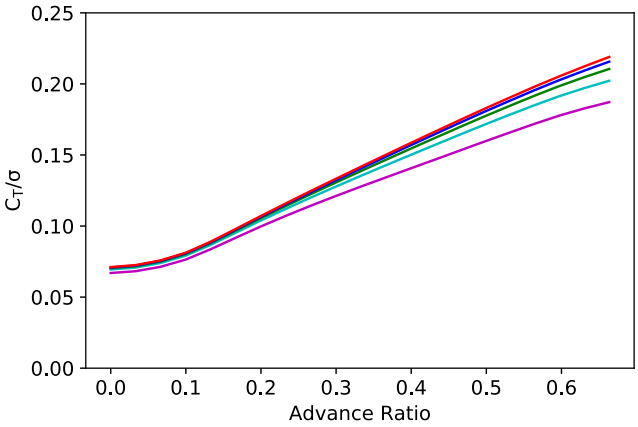

Figure 37. C_T/σ vs advance ratio (700 rpm), NACA 0012, five values of GJ

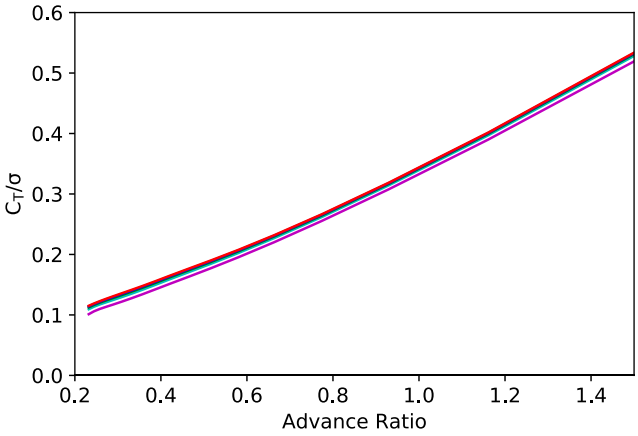

Figure 38. C_T/σ vs advance ratio (100 kts), NACA 0012, five values of GJ

NACA 0012 AIRFOIL, STABILITY ANALYSIS

Forward flight stability results are presented for the NACA 0012 in Figs. 39-40. In these figures, lines represent modes. With the nominal GJ value of 1000 lb-ft^2 and the nominal rotor speed of 700 rpm, the rotor does not flutter prior to 200

kts; however, this relatively high value is tempered by the fact that at a wind speed of 100 kts, flutter occurs at around 750 rpm, only slightly above the nominal value (Fig. 40). Thus, for an rpm-controlled configuration that will need to fly well above and below the nominal rotor speed, 150 kts will likely not be achievable. 100 kts is also likely overly ambitious, as it does not afford significant margin for rpm-control. A stiffer blade would be beneficial for stability; for blades analyzed with GJ of 2000-5000 lb-ft^2, flutter did not occur for any of the analyzed rpm/wind speed combinations. However, the previous section shows that there is a performance penalty associated with increased GJ, with stiffer blades stalling at lower advance ratios. Thus, there is a tradeoff between flutter speed and performance.

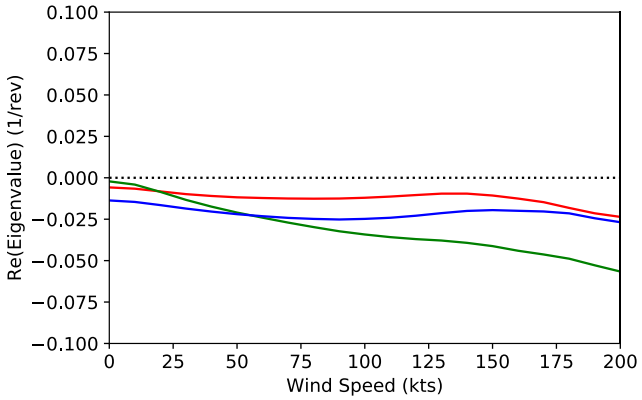

Figure 39. Stability vs wind speed, NACA 0012, GJ=1000 lb-ft^2

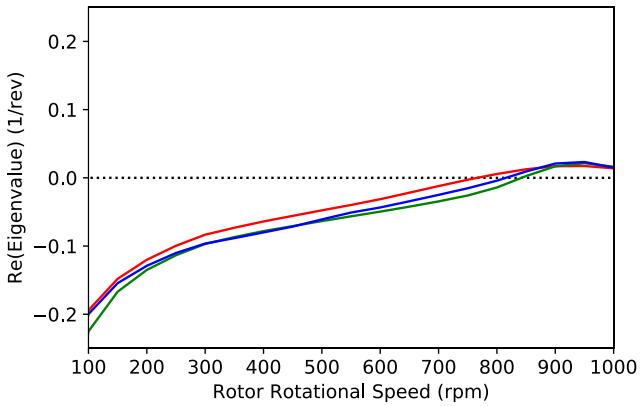

Figure 40. Stability vs rpm (100 kts), NACA 0012, GJ=1000 lb-ft^2

VR8 AIRFOIL, PERFORMANCE ANALYSIS

Figure 41 is a plot of Mean C_D vs advance ratio with rpm fixed at 700 (the legend of Fig. 41 applies to Figs. 41-44). Figure 42 again plots mean drag coefficient vs advance ratio, but with wind speed fixed at 100 kts and rpm swept through a 50:1500:50 sweep.

Figure 43 shows the relationship between thrust coefficient and advance ratio with rpm fixed at 700. Torsion stiffness has a significant effect on the nature of this relationship and upon the values of thrust coefficient. Figure 44 shows the relationship between thrust coefficient vs advance ratio at 100 kts. For this latter case, torsion stiffness has very little effect on both the nature of the relationship and on the values of thrust coefficient. Regarding Figs. 41-44, the differences yielded by different values of GJ are more substantial for the VR8 than for the analogous NACA 0012 cases.

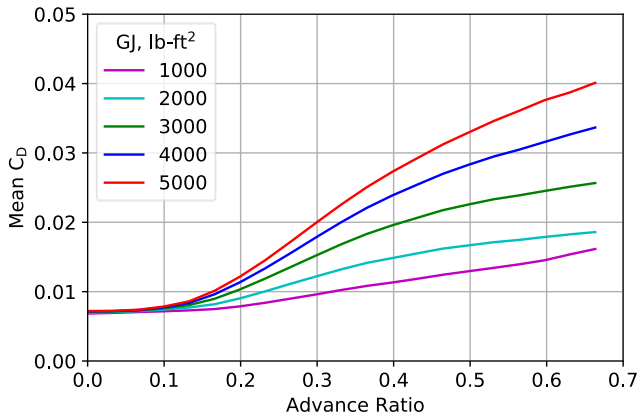

Figure 41. Mean C_D vs advance ratio (700 rpm), VR8, five values of GJ

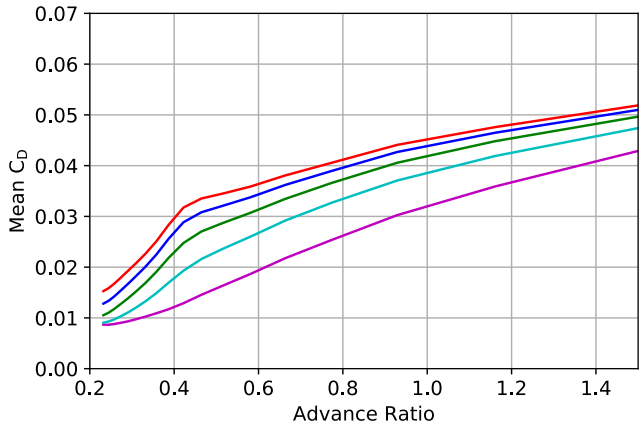

Figure 42. Mean C_D vs advance ratio (100 kts), VR8, five values of GJ

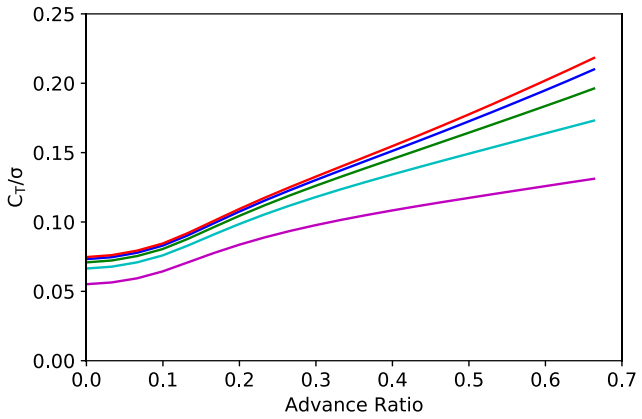

Figure 43. C_T/σ vs advance ratio (700 rpm), VR8, five values of GJ

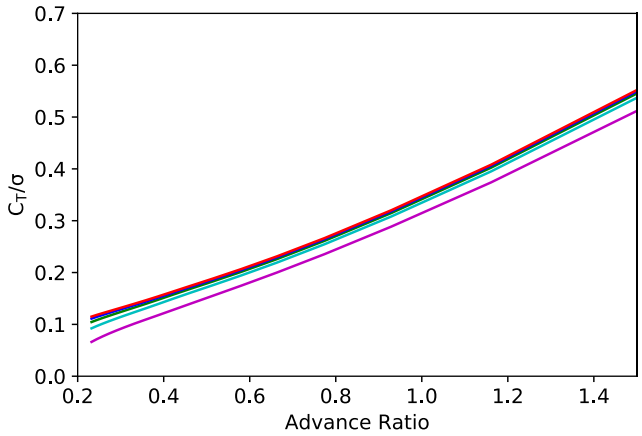

Figure 44. C_T/σ vs advance ratio, (100 kts), VR8, five values of GJ

VR8 AIRFOIL, STABILITY ANALYSIS

Forward flight stability results are presented for the VR8 (nominal GJ) in Figs. 45-46. In these figures, lines represent modes. Flutter did not occur for the cases analyzed with GJ values of 2000-5000 lb-ft^2. With nominal GJ and the nominal rotor speed of 700 rpm, the rotor flutters at approximately 150 kts; however, at 100 kts, flutter occurs at approximately 800 rpm. As with the NACA 0012, 100 kts is likely overly ambitious due to the small stability margin. A blade with higher torsion stiffness would be beneficial; however, as was noted for the NACA 0012, there is a tradeoff between stability and performance.

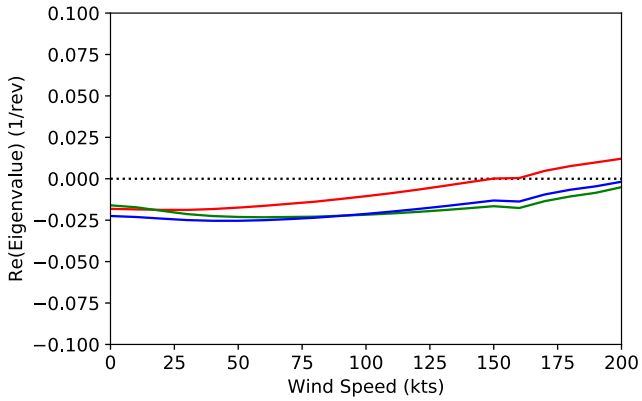

Figure 45. Stability vs wind speed (700 rpm), VR8, GJ=1000 lb-ft^2

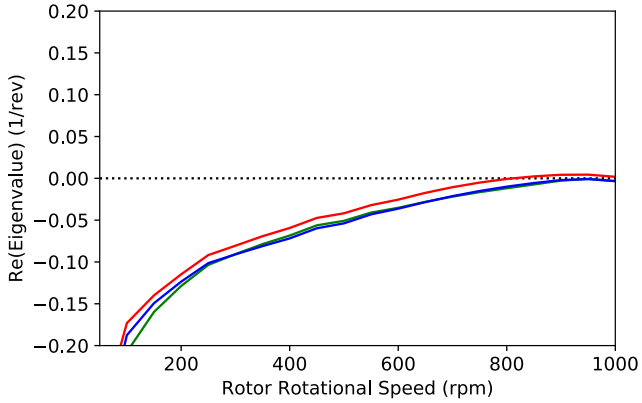

Figure 46. Stability vs rpm (100 kts), VR8, GJ=1000 lb-ft^2

VR12 AIRFOIL, PERFORMANCE ANALYSIS

Figure 47 is a plot of Mean $C_D$vs advance ratio with 700 rpm (the legend of Fig. 47 applies to Figs. 47-50). Figure 48 again plots mean drag coefficient vs advance ratio, but with 100 kts and rpm swept as 50:1000:50. As shown in Fig. 47, for the nominal values of GJ and rpm, significant stall was not built up within the analyzed range of wind speeds.

Figure 49 shows the relationship between thrust coefficient and advance ratio with rpm fixed at 700. Torsion stiffness has a significant effect on the nature of this relationship and upon the values of thrust coefficient. Figure 50 shows the relationship between thrust coefficient vs advance ratio at 100 kts. For this latter case, torsion stiffness has very little effect on both the nature of the relationship and on the values of thrust coefficient. As with the VR8, the differences yielded by different values of GJ are more substantial for the VR12 than for the analogous NACA 0012 cases.

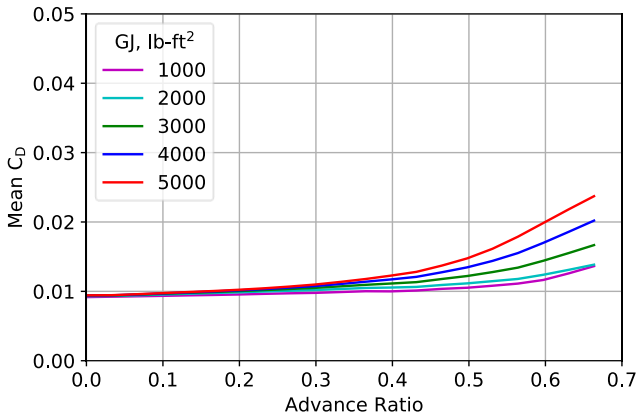

Figure 47. Mean C_D vs advance ratio (700 RPM), VR12, five values of GJ

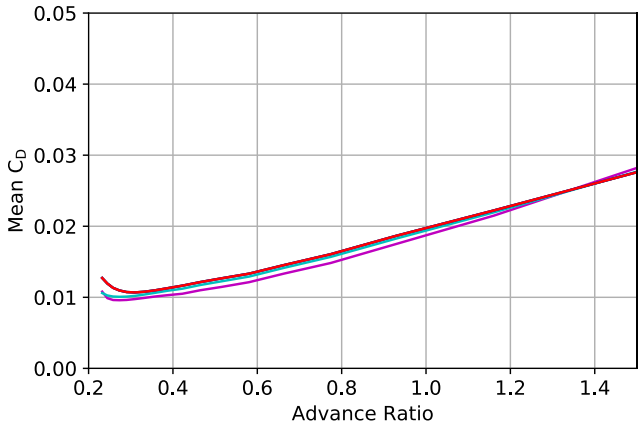

Figure 48. Mean C_D vs advance ratio (100 kts), VR12, five values of GJ

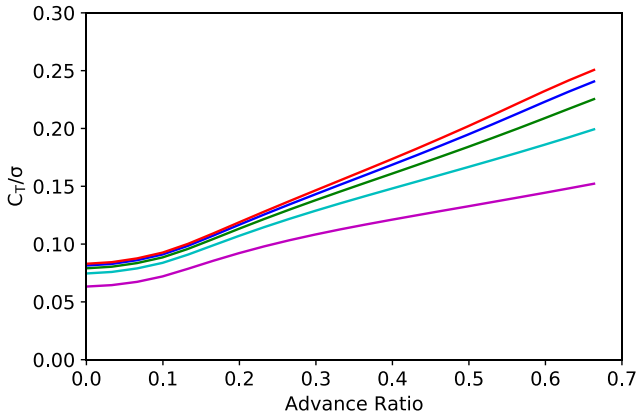

Figure 49. C_T/σ vs advance ratio (700 rpm), VR12, five values of GJ

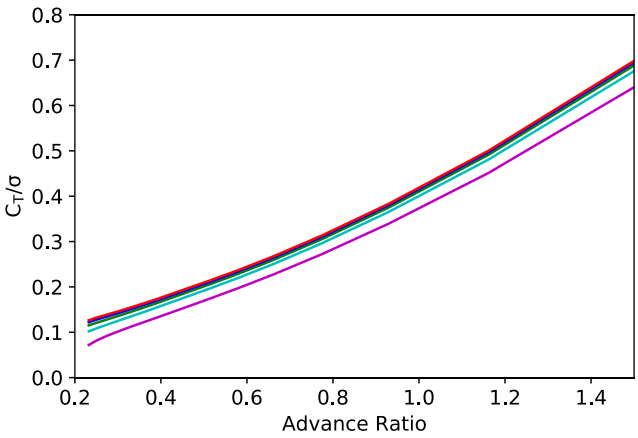

Figure 50. C_T/σ vs advance ratio (100 kts), VR12, five values of GJ

VR12 AIRFOIL, STABILITY ANALYSIS

Forward flight stability results are presented for the VR12 in Figs. 51-52. In these figures, lines represent modes. With the nominal GJ value of 1000 lb-ft^2 and the nominal rotor speed of 700 rpm, the rotor flutters at approximately 125 kts; however, at 100 kts, flutter occurs at approximately 775 rpm. Thus, for an rpm-controlled configuration that will need to fly well above and below the nominal rotor speed, 125 kts will likely not be achievable. 100 kts is also unachievable, as it does not afford significant margin for rpm-control. Cases analyzed with GJ of 2000-5000 lb-ft^2 did not flutter, showing that a stiffer blade would be beneficial for stability.

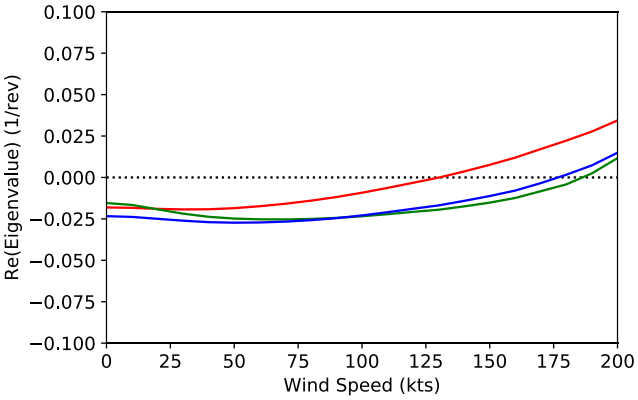

Figure 51. Stability vs wind speed (700 rpm), VR12, GJ=1000 lb-ft^2

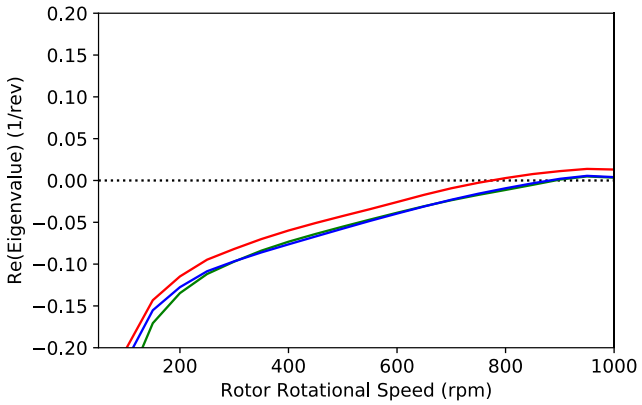

Figure 52. Stability vs rpm (100 kts), VR12, GJ=1000 lb-ft^2

FLOQUET ANALYSIS

In the field of rotorcraft aeromechanics, it is generally accepted that below an advance ratio of about 0.5 constant coefficient stability analysis yields acceptable results. This is the analysis method used in the previous section. However, beyond $\mu \approx 0.5$, constant coefficient analysis does not always yield sufficiently accurate results, and analysis with periodic coefficients via the invocation of Floquet Theory is necessary. The forward flight stability analysis of the previous section was repeated with Floquet Theory analysis for the purpose of verifying the results. Results were obtained via numerical integration. The Runge-Kutta integration method was employed with 300 time steps.

Due to agreement between the averaged results and the Floquet results, only the NACA 0012 cases were replicated. Results obtained via Floquet analysis for GJ values of 1000 and 5000 lb-ft^2 are presented in Figs. 53-56 and are overlaid with the constant coefficient results for the purpose of comparison. Results for GJ values of 2000-3000 lb-ft^2 were also generated but were omitted here for brevity. Note that in Fig. 53-56, the different lines of each analysis method represent the modes of the multiblade analysis.

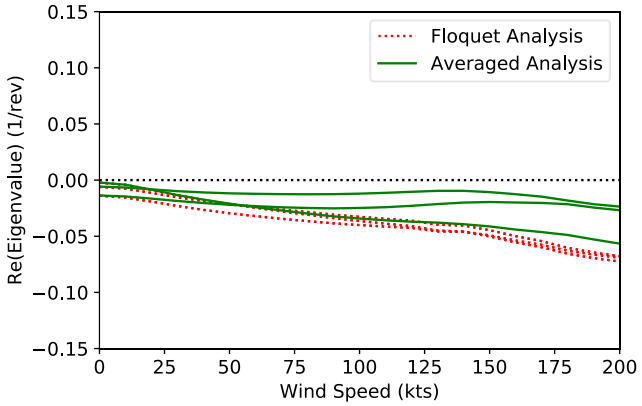

Figure 53. Stability vs wind speed (700 rpm), GJ =1000 lb-ft^2

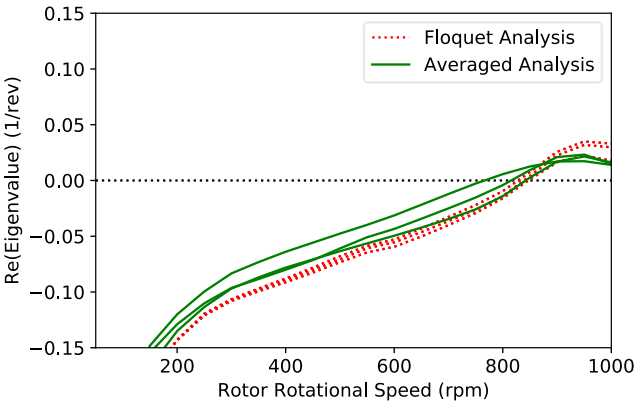

Figure 54. Stability vs rpm (100 kts), GJ=1000 lb-ft^2

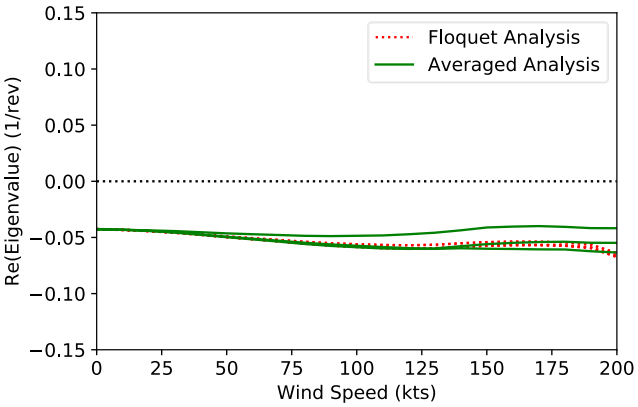

Figure 55. Stability vs wind speed (700 rpm), GJ=5000 lb-ft^2

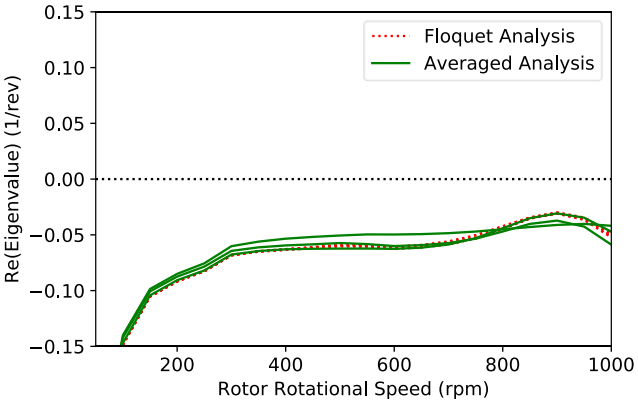

Figure 56. Stability vs rpm (100 kts), GJ=5000 lb-ft^2

FORWARD FLIGHT CONCLUSIONS

The results of the averaged analysis and the Floquet analysis were quite similar, and thus, in discussing forward flight conclusions, no distinction is made regarding a particular analysis method.

Table 9 summarizes the flutter speed at 700 rpm. Table 10 summarizes the flutter rpm at 100 kts. A dash in the flutter

speed column indicates that flutter did not occur within the analyzed range.

Table 9. Flutter Speed (kts) at 700 rpm

Airfoil	GJ (lb-ft^2)	Flutter Speed (kts)
NACA 0012	1000	-
NACA 0012	2000	-
NACA 0012	3000	-
NACA 0012	4000	-
NACA 0012	5000	-
VR8	1000	145
VR8	2000	-
VR8	3000	-
VR8	4000	-
VR8	5000	-
VR12	1000	135
VR12	2000	-
VR12	3000	-
VR12	4000	-
VR12	5000	-

Table 10. Flutter Speed (rpm) at 100 kts

Airfoil	GJ (lb-ft^2)	Flutter Speed (rpm)
NACA 0012	1000	775
NACA 0012	2000	-
NACA 0012	3000	-
NACA 0012	4000	-
NACA 0012	5000	-
VR8	1000	825
VR8	2000	-
VR8	3000	-
VR8	4000	-
VR8	5000	-
VR12	1000	775
VR12	2000	-
VR12	3000	-
VR12	4000	-
VR12	5000	-

Regarding performance, across all three airfoils (NACA 0012, VR8, and VR12), stall wind speed is lower for blades of higher torsion stiffness. For the NACA 0012 with GJ of 1000 lb-ft^2 and operating at 700 rpm, significant stall occurs at approximately $\mu = 0.6$. For the VR8 with GJ of 1000 lb-ft^2 and operated at 700 rpm, the rotor was not observed to stall below 200 kts; however, this is not the case for higher GJ values.

Regarding stability, across all three airfoils, flutter was only encountered with the nominal value of torsion stiffness (1000 lb-ft^2). For the NACA 0012 at the nominal rpm of 700, flutter was not encountered between 0 and 200 kts. For a fixed wind speed of 100 kts, flutter occurred at slightly beyond 700 rpm.

Overall, an inherent tradeoff between performance and stability was observed. More generally stated, trim and stall characteristics trade with GJ for stability. Stability is improved through increasing the GJ of the blades; however, it was observed that increasing GJ yielded a lower stall speed. A balance must be struck between the two criteria, resulting in a sufficiently stable configuration with a maximized stall speed.

CONCLUSIONS

A rotor model representative of a generic urban air mobility configuration was created and analyzed under a number of simulated conditions. Isolated rotor analysis was performed for both hover and forward flight. Airfoil, EA/CG location, GJ, rpm, and forward flight speed were parameters explored for their impact on performance and stability. The most notable observations are highlighted here.

Hover

1. There is significant coupling between torsion stiffness and stability; however, the strength of this coupling depends heavily on airfoil.
2. It is likely that if the EA/CG is at 35% chord, a much stiffer blade will be needed, regardless of airfoil. With this configuration of structural axes, none of the analyzed values of stiffness yielded a flutter point beyond the nominal rpm.

Forward Flight

1. Trim and stall characteristics trade with GJ for stability
2. Stability is improved through increasing the GJ of the blades; however, increasing GJ yields a lower stall speed.
3. Stability results obtained via the constant coefficient analysis were very similar to those obtained via Floquet Theory.

As mentioned previously, the work presented in this paper by no means represents a comprehensive examination of all relevant properties for a UAM rotor system. Rather, it is a preliminary study, aimed at providing an introductory understanding of the behavior of this type of rotor. Additional analysis will be necessary to gain a more complete picture of the problem. Future work will include the exploration of additional airfoils and additional blade stiffness properties. A wider range of the EA and CG offsets will be analyzed. Ultimately, analysis will move beyond an isolated rotor and will incorporate an airframe.

Author contact: Stephen Wright, sjwr@umich.edu

ACKNOWLEDGMENTS

With a full heart, I gratefully acknowledge my Aeromechanics family at NASA Ames Research Center. For their support, inspiration, motivation, and friendship over the years, I am deeply thankful. I specifically thank Wayne Johnson for his guidance, Ethan Romander for his assistance, and William Warmbrodt for his mentorship.

I thank Mizuho Takayama for her involvement in the early stages of this research.

Certain components of this research were undertaken while working full-time for NASA Ames Research Center. Other components of the research were conducted while at the University of Michigan as a Graduate Research Fellow of the National Science Foundation. Due to these latter components, the following acknowledgment and disclaimer apply:

This material is based upon work supported by the National Science Foundation Graduate Research Fellowship under Grant No. DGE 1841052. Any opinion, findings, and conclusions or recommendations expressed in this material are those of the author(s) and do not necessarily reflect the views of the National Science Foundation.

REFERENCES

1. Staruk, W., Butt, L., Hennig, G., Bonny, E., Gray C., Represa, D., Toner, R., "Wind Tunnel Testing and Analysis of a Rigid, Variable Speed Rotor for eVTOL Applications," Vertical Flight Society's 76th Annual Forum and Technology Display, Online, October 6-8, 2020.

2. Whittle, R., "Air Mobility Bonanza Beckons Electric VTOL Developers," *Vertiflite*, March/April 2017.

3. Swartz, K. I., "Charging Forward New eVTOL Concepts Advance," *Vertiflite*, July/August 2017.

4. Johnson, W., "Rotorcraft Aeromechanics Applications of a Comprehensive Analysis," HeliJapan 1998: AHS International Meeting on Rotorcraft Technology and Disaster Relief, Gifu, Japan, April 1998.

5. Silva, C., Johnson, W., and Solis, E., "Concept Vehicles for VTOL Air Taxi Operations," AHS Technical Meeting on Aeromechanics Design for Vertical Lift, Holiday Inn at Fisherman's Wharf, San Francisco, CA, January 16-18, 2018.

6. McCroskey, W. J., "A Critical Assessment of Wind Tunnel Results for the NACA 0012 Airfoil," NASA TM 100019, 1987.

7. Benson, G. R., Dadone, L. U., Gormont, R. E., and Kohler, G. R., "Influence of Airfoils on Stall Flutter Boundaries of Articulated Helicopter Rotors." Journal of the American Helicopter Society, 18:1 (January 1973).

8. Dadone, L. U., "Design and Analytical Study of a Rotor Airfoil," NASA CR 2988, 1978.

9. Vieira, B. A. O., and Maughmer, M. D., "Consideration of Dynamic Stall in Rotorcraft Airfoil Design." American Helicopter Society 71st Annual Forum, Virginia Beach, VA, May 2015.